Published in final edited form as:
Lab Chip. 2012 December 7; 12(23): . doi:10.1039/c2lc40515f.

Time Encoded Multicolor Fluorescence Detection in a Microfluidic Flow Cytometer†

Joerg Martini, **Michael I. Recht**, **Malte Huck**, **Marshall Bern**, **Noble Johnson**, and **Peter Kiesel**
Palo Alto Research Center, 3333 Coyote Hill Rd., Palo Alto CA 94304, USA.

Abstract

We describe an optical detection technique that delivers high signal-to-noise discrimination to enable a multi-parameter flow cytometer that combines high performance, robustness, compactness and low cost. The enabling technique is termed “spatially modulated detection” and generates a time-dependent signal as a continuously fluorescing (bio-) particle traverses an optical transmission pattern along the fluidic channel. Correlating the detected signal with the expected transmission pattern achieves high discrimination of the particle signal from background noise. Additionally, the particle speed and its fluorescence emission characteristics are deduced from the correlation analysis. Our method uses a large excitation/emission volume along the fluidic channel in order to increase the total flux of fluorescence light that originates from a particle while requiring minimal optical alignment. Despite the large excitation/detection volume (~ 1mm), the mask pattern enables a high spatial resolution in the micron range. This allows for detection and characterization of particles with a separation (in flow direction) comparable to the dimension of individual particles. In addition, the concept is intrinsically tolerant of non-encoded background fluorescence originating from fluorescent components in solution, fluorescing components of the chamber and contaminants on its surface. The optical detection technique is illustrated with experimental results on multi-color detection with a single large area detector by filtering fluorescence emission of different particles through a patterned color mask. Thereby the particles’ fluorescence emission spectrum is encoded in a time dependent intensity signal and color information can be extracted from the correlation analysis. The multicolor detection technique is demonstrated by differentiation of micro-beads loaded with PE and PE-Cy5 that are excited at 532 nm.

Introduction

Flow cytometers are standard tools in clinical diagnostics and biomedical research. They are indispensable for diagnosing cancer and infectious diseases as well as for the routine medical decision making for example in AIDS [treatment][1]. Medical or biochemical information is obtained by selectively binding fluorescent markers to bio particles of interest, for example, cells or sub-cellular complexes. As these tagged particles are transported in a fluid stream[2] they are enumerated and their fluorescent and light scattering properties are recorded by the flow cytometer. Commonly, the optical properties of labeled particles are detected by focused laser light that is directed in the path of the particle stream. This excitation region usually covers the lateral width of the flow channel and tens of microns in flow direction. Fluorescence and scattered light emanating from this region is

Fax: 650 812 4251; Tel: 650 812 4880; joerg.martini@parc.com.
†Published as part of a themed issue on optofluidics

collected by high numerical aperture optics, usually in a confocal configuration, and directed to various detectors. In order to avoid coincident detection of two or more particles in the excitation/detection region, its size has to be limited. Furthermore, the excitation and detection region have to be precisely aligned to each other and to the fluidic stream of particles. For reproducible fluorescence intensity determination, laser power has to be stable during the transit of a particle through the excitation region (typically a few microseconds). Today's commercial flow cytometers use up to four lasers and sometimes dozens of detection channels to allow for flexibility in the choices of assays and for simultaneous detection of several fluorescent labels and, therefore, biomarkers. Typically the excitation laser light is blocked from entering the optical detection path by spectrally selective filters. There are two common detection schemes for the spectral selection of fluorescence emission. The first scheme, realized for example in a Life Technologies Attune® flow cytometer, uses dichroic mirrors and bandpass filter combinations to select the spectral detection regions that are transmitted onto the different detectors, typically photo-multiplier tubes. The other spectrally resolving detection method use one or more dispersive elements such as prisms, for example in iCyt's hyperspectral flow cytometer, or gratings[3] and directs the fluorescence light to different positions on a detector array. The positions, and therefore the individual detectors, are correlated to specific spectral regions of the detected light.

The complex and alignment-sensitive designs of classical flow cytometers in combination with their use of relatively delicate detectors make it very challenging to fabricate small, sensitive, low cost and rugged instruments. However, in recent years a number of scaled-down classical flow cytometer instruments have been developed for special purposes. For example Partec's CyFlow® miniPOC, EMD Millipore's Muse Cell Analyzer or BD's FACSCount are marketed with an emphasis on small size and reduced cost. One main driver for this development is the urgent need to perform CD4 T-lymphocyte counts for screening, initiation of treatment, and monitoring of HIV-infected patients[4]. In the absence of centralized laboratories, particularly in the developing world, accurate point-of-need testing becomes essential and has triggered a variety of additional approaches for cell detection, example mechanical sensors, image cytometry and electrical detection as summarized by Boyle et al.[5].

Microfluidic flow cytometer concepts promise a combination of low cost, reduced size, ruggedness and therefore portability while permitting the use of standard assays and preventing cross contamination. Various publications[6-8] summarize competing fluidic, excitation and detection concepts and their implications for microfluidic flow cytometers' metrics. Generally, omitting or reducing the sheath flow of classical instruments relaxes the fluidic system requirements such as the number of pumps or the generation of waste. Some examples of cell positioning in fluidic channels include the streamline manipulation by mechanical structures in channels[9,10], the use of the fluid's inertia in shaped micro-channels[11-15] and their confinement by ultrasound effects[16]. Among other concepts that align the optic and fluidic paths[17,18] structuring waveguides and fluidic channels on the same chip[19-23] or embedding optical fibers into a fluidic chip[24-27] are a common approach to achieve alignment insensitivity. Fluorescence and scattered light can be directed through the same type of light guide as the excitation laser and subsequently wavelength filtered[28-30]. Other wavelength dependent detection concepts employ multiple filters and detectors along the fluidic path[31], detection of complete emission spectra[32,33], and microfluidically tunable filters[34]. Microfluidic-based flow cytometers have the fundamental advantage of easily replaceable fluidics to prevent cross contamination and enable waste storage on chip. In this paper we will describe a technique that is particularly suited for the design of alignment insensitive multi-color instruments, because the excitation spot can overfill the detection area. The detection area, on the other hand, is bonded to the

fluidic channel during the production process. Together, they allow for a very easily replaceable fluidic chip.

Measurement Concept

Unlike classical flow cytometers, our device uses a large area excitation and detection concept which makes the alignment of the system fundamentally more robust. Fluorescent particles are continuously excited while they travel through the excitation/detection zone of the fluidic chip. We can use high excitation intensities along the whole detection area because high power laser diodes and DPSS-lasers are relatively inexpensive for many popular excitation wavelengths. Thereby, we generate more fluorescence photons per particle than classical flow cytometers which results in improved photoelectron statistics. Due to fluorophore bleaching and saturation, conventional flow cytometers are limited to excitation intensities comparable to ours, but in much smaller excitation areas. To account for coincidence of several particles in the detection region, a mask of alternating transmissive and opaque regions transmits and blocks the fluorescence light emanating from particles flowing in a microfluidic channel (see figure 1 A).

As the particles flow by the mask with constant speed, the transmission of the continuous fluorescence light to the detector is interrupted by the transmission mask. In other words, as the spatial pattern of the mask modulates the detected fluorescence light of a moving particle in time, it generates a “blinking pattern” (see figure 1B). Hence, we term our enabling technique “spatially modulated detection”.

It is important to note that background signal, originating for example from contaminants in the fluidic channel or unbound dye, does not affect our system significantly. Our background signal is increased compared to classical confocal detection concepts due to the larger excitation/detection area. However the mean background value is subtracted from the data stream. The noise of the background only increases with the square root of the background signal. At the same time the total signal increases just as much as the background. In contrast to background signal, light form target objects shows characteristic time modulation due to their relative movement with regard to the mask pattern. Both effects result in an improved signal-to-noise ratio in the system.

To determine the number, speed and intensity of particles in the detection region we “look for” the characteristic time trace of a fluorescing particle in the continuous fluorescence intensity signal. The time trace is represented by the spatial mask pattern, and its duration is particle speed dependent.

Mathematically the match of a particle’s recorded and expected signal can be calculated by the correlation integral:

$$C(t, v_n) = \int_{-T/2}^{T/2} M(v_n, \tau)\, S(\tau + t)\, d\tau \quad (1)$$

where $M(v_n,t)$ is the spatial transmission pattern, $S(t)$ is the recorded fluorescence intensity signal, and τ is the length of the examined signal. The calculation is performed over a range of particle speeds v_n.

At time t_p a particle of the speed v_{corr} is detected with Eq. 1 when $C(t_p,v_{corr})$ shows a local maximum which is usually very clearly pronounced. Therefore a peak detection algorithm on the derivative of Eq. 1 can be used to determine t_p and v_{corr}. Then $C(t_p,v_{corr})$ is a measure for the fluorescence intensity of the particle. This basic concept, its lab implementation, and first proof-of-concept demonstration are described in Kiesel et al.[35]. As the fluorescence

signal S(t) is discretely sampled by an analog-to-digital converter, we replace the integral in Eq. 1 by summing discrete signal data points S_i with discrete mask representation data points $M_i(v_n)$.

$$C(t, v_n) = \sum_{i}^{\tau} S_{t+i} \cdot M_{t+i}(v_n) \quad (2)$$

For the evaluation of these datasets we typically probe the dot-product of Eq. 2 over a range of selected particle speeds v_n, the maximum value of C identifying the particle speed v_{corr}.

It is important to note that the background signal, in particular unbound dye, is not modulated by the mask because it is continuously present in the detection area. Therefore it does not exhibit the characteristic blinking pattern but a DC-offset that is subtracted from S_i to prevent its contribution to the correlation value. Noise in the background signal does generally not correlate with the expected signal $M_i(v_n)$ and therefore is not wrongfully registered as a particle of weak intensity.

The emission mask and the fluidic channel are aligned and bonded together during fabrication of the fluidic channel. Therefore, the alignment of the system is performed during the manufacturing of the disposable fluidic chips. The exciting light spot can then be larger than the detection area because excess excitation light is blocked by the mask.

The design of the transmission mask pattern is application specific. For high particle concentration, when several particles are expected in the detection region, a pseudo-random mask pattern with minimal self-similarities is advised. Mask patterns with self-similarities should be avoided, because they lead to multiple correlation maxima (see Eq. 1) per particle. The minimum feature size of the mask determines roughly the spatial resolution of the whole detection region and is typically chosen to be slightly larger than the particles of interest.

In a prototype hand-held setup (see figure 2A) we tested this measurement and data acquisition concept. The setup uses a low-cost 100mW 532 nm laser for excitation and a silicon based photomultiplier for detection. Fluorescence light is collected with a high numerical aperture lens and directed through a 535 nm longpass and a 585/40 nm bandpass filter onto the detector. The fluidic chip consists of a metalized quartz slide with the spatial mask pattern bonded to a light guiding PMMA top. The height of the fluidic channel is ca. 25μm while the planar dimensions of the detection area are typically 1.2mm (in flow direction) by 100μm[36] as defined by the mask.

We have evaluated the sensitivity and detection range of our prototype with various calibration particles. These are small-diameter beads impregnated with a specific fluorophore to a known concentration[37]. Fig 2 shows results for 2μm Rainbow calibration (RCP-20-5, Spherotech) which contains four subpopulations of beads with different brightness. Fig 2B shows the speed profile and Fig. 2C the intensity histogram. The speed of the particles is distributed between approximately 0.5 and 1.1m/s. The absolute calibration of the intensity axis in MEPE (“molecules of equivalent PE”) was obtained by cross calibration with commercially available calibration beads with exact specified number of PE (Phycoerythrin) dye (BD Quantibrite, BD Biosciences). Our measurement shows that we clearly resolve all 4 peaks. The detection limit of this prototype is about 50 MEPE which exceeds the sensitivity of some commercially available high-end instruments.

Remote sensing

Instead of permanently aligning the transmission mask with the fluidic channel, as in the prototype instrument discussed above, it is also possible to image an unobstructed channel onto a transmission mask in front of the detector. Due to the high NA of the collection lens, the channel image is then usually magnified. To ensure optimal spatial modulation, the channel needs to be correctly focussed on the mask. In a test setup this is advantageous because it allows for rapid changing of the mask pattern, and it provides the possibility of filtering the laser light before the mask. In addition, remote masks are easier to fabricate than direct masks, because they are larger and they do not need to be water resistant.

Periodic Masks

In the example above we used a pseudo-random mask pattern which allows distinguishing and separating signals from multiple particles that are simultaneously in the detection area. For a number of flow cytometer applications that seek to identify comparatively rare particles, a periodic transmission mask is an appropriate alternative choice. Rather than the dot-product for different particle speeds, a fast Fourier transformation (FFT)[38] of the fluorescence intensity signal is calculated. This accelerates the data evaluation, produces accurate speed information, and ensures a very reliable signal discrimination from the noise[39]. With FFT of the fluorescence intensity, a particle is identified by a distinct frequency peak due to the periodic transmission and blocking of the light when the particle passes the mask. For example, a mask with transparent stripes of 25μm width followed by 25 μm wide opaque stripes generates a FFT peak at 20 kHz when particles are traveling at 1 m/s and 16 kHz when they are traveling at 0.8 m/s. Therefore, several particles that flow through the detection region simultaneously can only be identified if they significantly differ in speed. In order to avoid particle-wall interactions and channel clogging we use a two-dimensional sheath-flow in our system which effectively dilutes the analyte concentration. The probability to encounter more than one particle in the detection zone can be calculated by the Poisson distribution. For instance with an analyte-to-sheath ratio of ~30 we encounter particle coincidences with 1% probability only at concentrations > 1600 particles/μl, which is, for example, sufficient to determine CD4 T-lymphocyte counts for HIV monitoring[40].

Patterned Color Masks

In order to expand the versatility of our approach to multicolor detection, we created structured color masks[41] with spectrally selective transparent regions. We alternated for example filter regions that are transparent to a first fluorophore and opaque to another fluorophore, with filter regions of the reverse spectral transmission characteristic. Thereby inverted fluorescence signals for the two fluorophores[39] are generated. This approach requires non-periodic masks and a data evaluation that uses the correlation analysis of Eq. 2 with two mask functions that represent the two transmission characteristics of the mask. While a particle with the fluorescence characteristics of the first fluorophore shows a maximum in the correlation value at time t_p and speed v_{corr} for its respective mask function, its correlation value is ideally zero for the complementary mask function. The second fluorophore exhibits the inverted behavior. Therefore the correlation values of the two mask functions represent the relative abundance of the two fluorophores. In another approach, we can use different spatial frequencies of particular color filters to infer from the FFT signal which fluorophore is present. However, with variable particle speeds, the FFT frequency alone is not sufficient to uniquely correlate them to a particular fluorophore. Therefore, we use color filters/fluorophore combinations with overlapping spectral characteristics. A given fluorophore then exhibits more than one FFT peak. Their relative height to one another identifies the fluorophore, while the ratio of detected FFT peak frequencies is determined by the mask design.

Experimental Setup

For multicolor detection we altered our detection scheme as described above by using an unobstructed detection area of 1 mm × 100 μm that is imaged onto a color mask. The masks consisted of areas with varying spectral transmission characteristics. The parts of the mask that are transparent between 510 nm and 570 nm will be referred to as “green”, areas that have a 510 nm longpass characteristic as “yellow” and the ones that have a 610 nm longpass characteristic as “red”. Additionally, the color masks have opaque regions, depicted in “black”. In front of this mask is a 532 nm longpass filter to block incident laser light. An additional focusing lens directs light that is transmitted through the mask onto the detector. The fluorescence signal was recorded at 200000 samples/s with an analog-to-digital converter and subsequently analyzed with a MATLAB evaluation program. This software calculates the FFT for 3000 subsequent data points detects FFT peaks and evaluates their height and frequency position. The intensity of the particle is calculated by the dot-product of expected and detected signal and subsequently normalized by the particle speed to represent the particle’s inherent fluorescence properties, independent of its dwell-time in the excitation/detection area.

Results

Adjacent Patterns

We implemented a multicolor detection scheme by placing two periodic masks of different periodicity sequentially in flow direction. The first part transmits in the “red” spectral region while the second part transmits “green”. The ratio of periodicities between both sides is 3-to-4. Figure 4A (top) illustrates this mask and presents the fluorescence signal of two different beads. The red time trace shows the fluorescence intensity characteristics of a PE-Cy5 fluorescence particle (ECFP-F4-5K, Spherotech) passing by the transmission mask. PE-Cy5 predominantly emits between 650 and 700 nm. Similarly, the green time trace shows the fluorescence intensity characteristics of a PE fluorescence particle (ECFP-F2-5K, Spherotech), which predominantly emits between 550 and 600 nm but has a significant emission tail up to 650nm Both fluorescence time traces show an overall Gaussian-shaped intensity envelope which is due to the laser intensity distribution along the channel. It should be noted that Fig. 4 does not depict particles that were recorded simultaneously. Signals from two separate particles with approximately identical speed and brightness were selected and superimposed to illustrate the signal difference due to their spectral emission characteristics. While PE-particles show a significant crosstalk in the red channel, PE-Cy5 emission is hardly discernable in the green channel. The FFT evaluations of both particles (Fig. 4 B) correspond to this observation. While the PE-Cy5 particle generates a very dominant frequency peak at 16 kHz it does not generate a significant one at higher frequencies, which indicates that there is little transmission in the green channel. The PE-particle on the other hand shows two distinct FFT peaks with approximately the expected frequency ratio of ¾. In other words, the crosstalk of PE into the red channel can provide the identifying FFT characteristic of PE versus PE-Cy5.

Interdigitated periodic patterns

To increase the transmissive area of the mask, we have also demonstrated the superposition of two periodic red and green masks, which, for example, have 33 and 23 transmission periods, respectively. The superposition adds the transmission of red and green to yellow (see Figure 5 A top), which is transparent for both PE and PE-Cy5 fluorescence emission. Both types of beads show clearly distinguishable fluorescence time patterns. The spectral characteristic of PE-Cy5 shows a clear periodic pattern due to the fact that the red and yellow transmission regions of the mask are equally transmissive. The PE spectral characteristic is more complex because it is transmitted in all channels with different

intensities. Accordingly, the FFT signal of a PE-Cy5 particle once more shows one distinct peak (Figure 5A, red FFT) while PE now exhibits three peaks. The two strong peaks at 23kHz and at 16 kHz for the selected particle in Figure 5A are associated with the initial ratio of transmission mask periods, here 23-to-33 (16kHz≈23/33·23kHz), while the third one is the beat frequency of the superposition, here 7kHz.

The fixed frequency relationships among the FFT peaks provide a criterion to categorize particles. In the example in Fig. 5, for a given detected FFT peak, the algorithm calculates FFT values at frequencies $f = 23/33 \cdot f_{peak}$ and $f = 33/23 \cdot f_{peak}$. After comparing the corresponding three FFT power density values, the two highest values are assigned to "red" (PD_{33}) at the higher frequency (f_{33}) and "green" (PD_{23}) at the lower frequency (f_{23}). The ratio of these power density values then provides a useful spectral characterization of PE and PE-Cy5 particles. Figure 5B shows a data set of a particle mixture that consists of Spherotech PE and PE-Cy5 beads with intensities of 15000 and 50000 MEPE for the PE particles and 390000 and 2200000 MEPE-Cy5 for the PE-Cy5 beads. The two types of particles are separated by a factor of 35 on the ordinate that is a measure for the spectral separation. The classification and color representation of particles is based the PD_{23}/PD_{33} power density ratios of the particles. Particles of $PD_{23}/PD_{33} > 0.2$ are classified as PE-beads while others are classified as PE-Cy5 particles. The average PD_{23}/PD_{33} value (± standard deviation) for PE particles is 1.2 ± 0.27 compared to 0.034 ± 0.02 for PE-Cy5 particles. The particles' intensity distributions and histograms are plotted along the abscissa, clearly separating the different intensities of the beads. In addition to the spectral and intensity information the detection method also provides the speed information of individual particles. In this measurement particle speeds ranged between 0.48m/s and 0.86m/s, averaging 0.66m/s.

Discussion and Conclusions

The particular strengths of our spatial modulation technique are its simplicity, robustness and alignment insensitivity. We extended the technique to include multi-color detection in order to retain these advantages when multiple fluorescence channels are to be recorded as required in many real world applications. To realize multi-color detection without the cost and complexity of multiple detectors and dichroic mirrors in a robust system, we conceptualized and developed an effective solution of encoding color information in the time domain[42]. At least one other group also uses a similar color detection schemes that time-encodes spectral information of moving particles by spatially separated filters[43]. While our interdigitated periodic patterns use ca. 50% of the available detection area for each of the two colors, this system is more comparable to our implementation of adjacent patterns which has a significantly lower active detection area per fluorophore, in our case ca. 25%. Using alternating filter characteristics and non-periodic patterns utilizes the complete detection area but requires a more complex detection and characterization algorithm. This approach is beneficial compared to interdigitated masks and FFT evaluation if coincidences of particles in the detection zone are frequent due to high particle concentrations. When using FFT evaluation, we seek to maintain a <1% probability for coincidences by adjusting the sheath-to-analyte ratio. For typical masks and flow rates this translates into maximum particle concentrations of ca. 1600 particles/μl.

Here we demonstrate a limit of detection of approximately 15000 MEPE and 390000 MEPE-Cy5, predominantly limited by relatively poor transmission (<40%) of the filter mask, in combination with fluorophore characterization. The average values of the PD_{23}/PD_{33} ratio, the measure for fluorophore characterization, are separated by more than three standard deviations. That means that more than 99% of particles are characterized correctly, which makes this technique suitable for relatively low particle densities. The clear

separation of PE and PE-Cy5 is a promising indication that the combined abundance of different fluorophores in or on a single particle can be resolved in our system. We use a patterned color mask that allows spectral detection with a single detector, maintaining the features of simplicity, low-cost and ruggedness of our device. This is achieved by translating the spectral particle information into varying time sequences for subsequent computational analysis of the data. The choices of mask patterns and spectral transmission characteristics have a significant influence on the data evaluation procedures. By choosing periodic mask patterns, the data evaluation is significantly accelerated with FFT-based data evaluation. Crosstalk between different fluorescence channels is commonly avoided in fluorescence detection by using high-end filters. In our system crosstalk provides the differentiator in the FFT signal for PE and PE-Cy5, making the use of low-end fluorescence filter not only possible but beneficial.

Acknowledgments

The work on the spatial modulation technique and its application in flow cytometry was partially supported by grants from the National Institute of Health (5R21EB011662-02) and the US Army Research Office (W911NF-10-1-0479).

References

[1]. Carey, J.; McCoy, J.; Keren, D. Flow Cytometry in Clinical Diagnosis. American Society for Clinical Pathology; 2007.

[2]. Shapiro, HM. Practical Flow Cytometry. John Wiley & Sons, Inc.; 2003.

[3]. Gregori G, Patsekin V, Rajwa B, Jones J, Ragheb K, Holdman C, Robinson JP. Cytometry A. 2012; 81(1):35–44. [PubMed: 22173900]

[4]. Antiretroviral Therapy for HIV Infection in Adults and Adolescents. Recommendations for a Public Health Approach. 2006. http://www.who.int/hiv/pub/guidelines/artadultguidelines.pdf

[5]. Boyle DS, Hawkins KR, Steele MS, Singhal M, Cheng X. Trends Biotechnol. 2011

[6]. Kim, JS.; Ligler, FS. The Microflow Cytometer. Pan Stanford Publishing Pte. Ltd.; 2010.

[7]. Ateya DA, Erickson JS, Howell PB Jr. Hilliard LR, Golden JP, Ligler FS. Anal Bioanal.Chem. 2008; 391(5):1485–1498. [PubMed: 18228010]

[8]. Godin J, Chen CH, Cho SH, Qiao W, Tsai F, Lo YH. J Biophotonics. 2008; 1(5):355–376. [PubMed: 19343660]

[9]. Thangawng AL, Kim JS, Golden JP, Anderson GP, Robertson KL, Low V, Ligler FS. Anal Bioanal.Chem. 2010; 398(5):1871–1881. [PubMed: 20658281]

[10]. Yun H, Bang H, Min J, Chung C, Chang JK, Han DC. Lab on a Chip. 2010; 10(23):3243–3254. [PubMed: 20941407]

[11]. Di CD, Edd JF, Humphry KJ, Stone HA, Toner M. Phys.Rev Lett. 2009; 102(9):094503. [PubMed: 19392526]

[12]. Hur SC, Tse HT, Di Carlo D. Lab on a Chip. 2010; 10(3):274–280. [PubMed: 20090998]

[13]. Di CD. Lab on a Chip. 2009; 9(21):3038–3046. [PubMed: 19823716]

[14]. Bhagat AA, Kuntaegowdanahalli SS, Kaval N, Seliskar CJ, Papautsky I. Biomed Microdevices. 2010; 12(2):187–195. [PubMed: 19946752]

[15]. Oakey J, Applegate RW Jr. Arellano E, Di CD, Graves SW, Toner M. Anal Chem. 2010; 82(9): 3862–3867. [PubMed: 20373755]

[16]. Goddard GR, Sanders CK, Martin JC, Kaduchak G, Graves SW. Anal Chem. 2007; 79(22):8740–8746. [PubMed: 17924647]

[17]. Schmidt H, Hawkins AR. Microfluid.Nanofluidics. 2008; 4(1-2):3–16. [PubMed: 21442048]

[18]. Hawkins AR, Schmidt H. Microfluid.Nanofluidics. 2007; 4(1-2):17–32. %19. [PubMed: 21603122]

[19]. Godin J, Lo YH. Biomed Opt.Express. 2010; 1(5):1472–1479. [PubMed: 21258563]

[20]. Jensen TG, Nielsen LB, Kutter JP. Electrophoresis. 2011; 32(10):1224–1232. [PubMed: 21500210]

[21]. Lunt EJ, Wu B, Keeley JM, Measor P, Schmidt H, Hawkins AR. IEEE Photonics Technol.Lett. 2010; 22(15):1147–1149. [PubMed: 21423839]

[22]. Lunt EJ, Measor P, Phillips BS, Kuhn S, Schmidt H, Hawkins AR. Opt.Express. 2008; 16(25): 20981–20986. [PubMed: 19065238]

[23]. Schonbrun E, Steinvurzel PE, Crozier KB. Optics Express. 2011; 19(2):1385–1394. [PubMed: 21263680]

[24]. Rosenauer M, Vellekoop MJ. Biomicrofluidics. 2010; 4(4):43005. [PubMed: 21267437]

[25]. Kennedy MJ, Stelick SJ, Sayam LG, Yen A, Erickson D, Batt CA. Lab Chip. 2011; 11(6):1138–1143. [PubMed: 21279198]

[26]. Schafer D, Gibson EA, Salim EA, Palmer AE, Jimenez R, Squier J. Optics Express. 2009; 17(8): 6068–6073. [PubMed: 19365429]

[27]. Hashemi N, Erickson JS, Golden JP, Ligler FS. Biomicrofluidics. 2011 (in press).

[28]. Golden JP, Kim JS, Erickson JS, Hilliard LR, Howell PB, Anderson GP, Nasir M, Ligler FS. Lab Chip. 2009; 9(13):1942–1950. [PubMed: 19532970]

[29]. Tung YC, Zhang M, Lin CT, Kurabayashi K, Skerlos SJ. Sensors and Actuators B: Chemical. 2004; 98(2â€“3):356–367.

[30]. Hashemi N, Erickson JS, Golden JP, Jackson KM, Ligler FS. Biosens.Bioelectron. 2011; 26(11): 4263–4269. [PubMed: 21601442]

[31]. Grafton, MMG.; Maleki, T.; Zordan, MD.; Reece, LM.; Byrnes, R.; Jones, A.; Todd, P.; Leary, James F.; Byrnes, R.; Jones, A.; Todd, P. Proc.SPIE 7929. Vol. Volume 7929. Microfluidics, BioMEMS, and Medical Microsystems IX; Techshot, Inc.; USA: 2011. Microfluidic MEMS hand-held flow cytometer. 79290C-79290C-10

[32]. Shi-Wei, Lin; Chih-Han, Chang; Chia-Yen, Lee; Lung-Ming, Fu; Che-Hsin, Lin. Sensors. IEEE; Nov 1. 2010 Novel flow cytometrer utilizing wavelength-resolved detection under a diascopic illumination configuration. 1987-19902010

[33]. Huang NT, Truxal SC, Tung YC, Hsiao AY, Luker GD, Takayama S, Kurabayashi K. Anal Chem. 2010; 82(22):9506–9512. [PubMed: 20979407]

[34]. Measor P, Phillips BS, Chen A, Hawkins AR, Schmidt H. Lab Chip. 2011; 11(5):899–904. [PubMed: 21221449]

[35]. Kiesel P, Bassler M, Beck M, Johnson N. Appl.Phys.Lett. 2009; 94(4):041107–3.

[36]. Kiesel P, Martini J, Beck M, Huck M, Bern MW, Johnson NM. Laser Focus World. 2010; 15(10):47–50.

[37]. Hoffman, RA. Standardization and Quality Assurance in Fluorescence Measurements II. In: Resch-Genger, U., editor. Flow Cytometry: Instrumentation, Applications, Future Trends and Limitations. Springer; Berlin Heidelberg: 2008.

[38]. Cooley JW, Tukey JW. Math.Comp. 1965; 19:297–25. 301.

[39]. Kiesel, P.; Martini, J.; Huck, M.; Johnson, NM.; Bern, MW.; Recht, MI. Point of care Diagnostics on a Chip. In: Westervelt, RM.; Issadore, D., editors. Flow Cytometry on a Chip. Springer; 2012.

[40]. Boyd SD. Am J Health Syst.Pharm. 2011; 68(11):991–1001. [PubMed: 21593227]

[41]. Bassler, M.; Kiesel, P.; Beck, M.; Hegyi, A.; Bruegel, T.; Johnson, NM. US 7,894,068, Producing Filters with Combined Transmission and /or Reflection Functions. Feb 22. 2011

[42]. Bassler M, Beck M, Kiesel P, Hegyi A, Bruegel T, Johnson NM. US 7,701,580, Transmitting/ Reflecting Emanating Light with Time Variation. Apr 20.2010

[43]. Cho SH, Qiao W, Tsai FS, Yamashita K, Lo YH. Appl.Phys.Lett. 2010; 97(9):093704. [PubMed: 20877655]

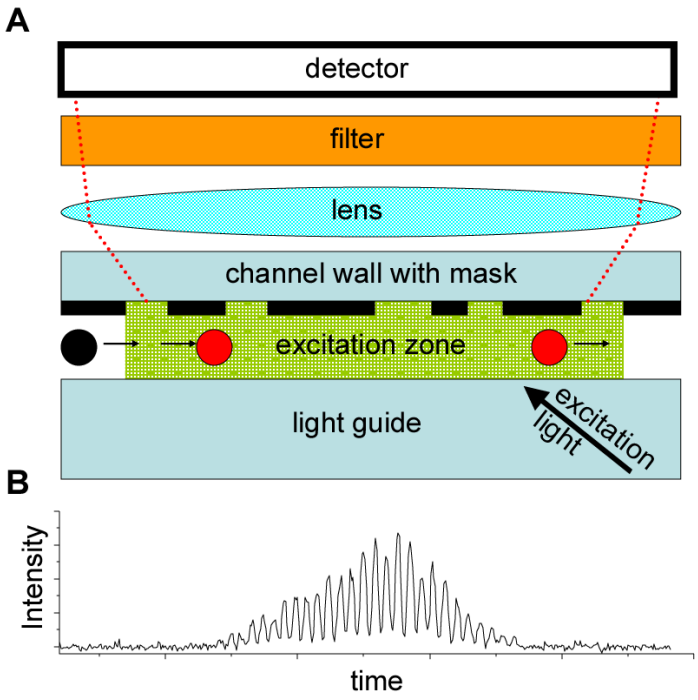

Fig. 1.
schematic detection concept: A) fluorescence of particles is generated in the excitation zone by laser light and detected through a spatial mask and filter B) the linear movement of the particle relative to the patterned transmission mask results in a characteristic temporal modulation of the fluorescence intensity that is detected

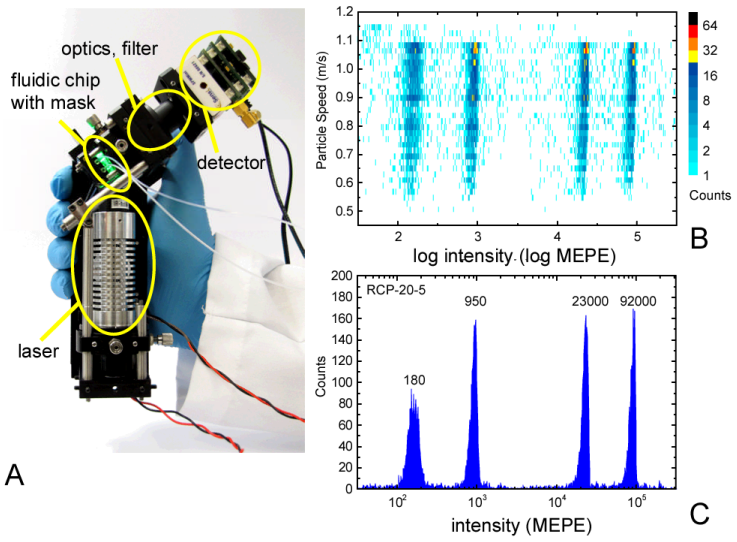

Fig. 2.

A) handheld prototype setup b) fluorescence intensity vs. speed histogram, absolute counts of Spherotech calibration particles (RCP-20-5) are color encoded C) fluorescence intensity histogram of Fig. 2 C, the measured fluorescent intensities for all peaks are in excellent agreement with the nominal values.; fluorescence intensity in B) and C) presented in molecules of equivalent Phycoerythrin

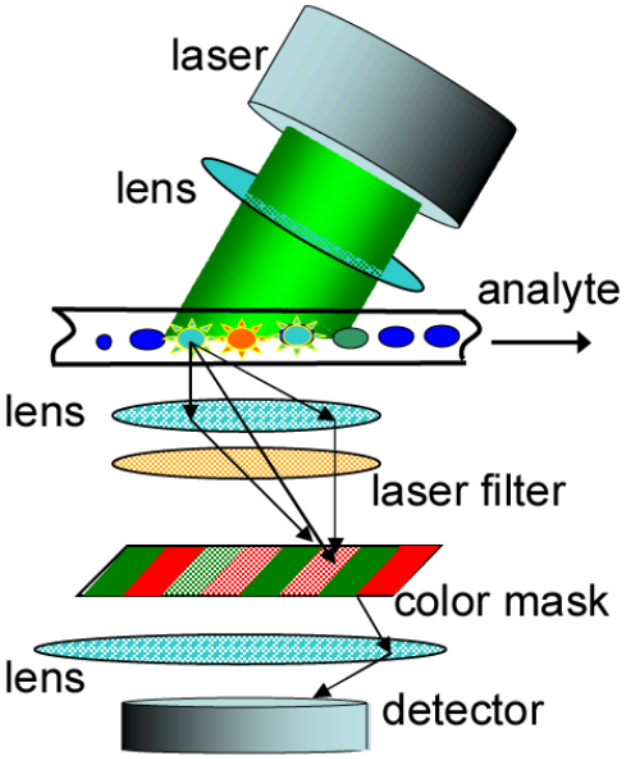

Fig. 3.
schematic setup of remote sensing approach

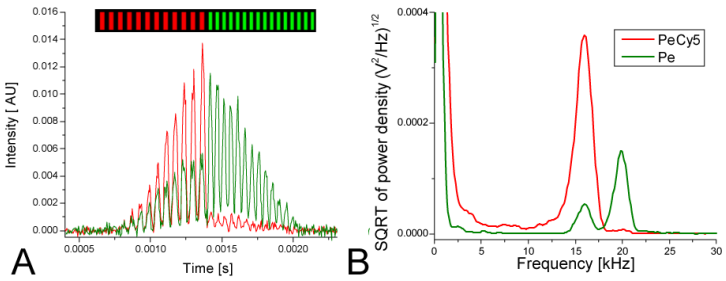

Fig.4.

A) pattern of spatial color mask on top and fluorescence intensity signal of PE (green) and PE-Cy5 (red) particle B) FFT of A)

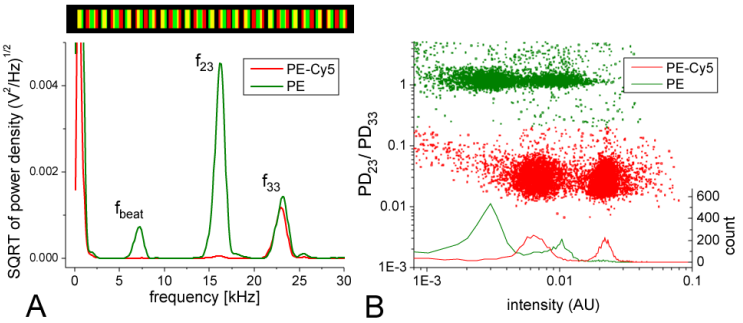

Fig.5.

A) transmission mask design (top) that results in a 33-to-23 frequency ratio (f_{23} and f_{33}) for the two largest FFT peaks of a PE particle as well as a beat frequency peak (f_{beat}). PE-Cy5 particles show only one pronounced peak at frequency f_{33} B) spectral and intensity separation of PE (intensities ca. 50000 and 15000 MEPE) and PE-Cy5 (intensities ca. 390000 and 2200000 MEPE-Cy5) particle mixture including intensity histogram of the particles.